AD-A036 501

AFWL SCANNING INTERFEROMETER

Air Force Weapons Laboratory
Kirtland Air Force Base, New Mexico

January 1977

AFWL SCANNING INTERFEROMETER

January 1977

Final Report

Approved for public release; distribution unlimited.

AIR FORCE WEAPONS LABORATORY
Air Force Systems Command
Kirtland Air Force Base, NM 87117

REPORT DOCUMENTATION PAGE		READ INSTRUCTIONS BEFORE COMPLETING FORM
1. REPORT NUMBER AFWL-TR-76-268	2. GOVT ACCESSION NO.	3. RECIPIENT'S CATALOG NUMBER
4. TITLE *(and Subtitle)* AFWL SCANNING INTERFEROMETER		5. TYPE OF REPORT & PERIOD COVERED Final Report
		6. PERFORMING ORG. REPORT NUMBER
7. AUTHOR(s) Dave Holmes Burton D. O'Neil, Major, USAF Roy L. Parnell, Captain, USAF		8. CONTRACT OR GRANT NUMBER(s)
9. PERFORMING ORGANIZATION NAME AND ADDRESS Air Force Weapons Laboratory (LRO) Kirtland Air Force Base, NM 87117		10. PROGRAM ELEMENT, PROJECT, TASK AREA & WORK UNIT NUMBERS 63000F 00011497
11. CONTROLLING OFFICE NAME AND ADDRESS Air Force Weapons Laboratory Kirtland AFB, NM 87117		12. REPORT DATE January 1977
		13. NUMBER OF PAGES 38
14. MONITORING AGENCY NAME & ADDRESS*(if different from Controlling Office)*		15. SECURITY CLASS. *(of this report)* Unclassified
		15a. DECLASSIFICATION/DOWNGRADING SCHEDULE

16. DISTRIBUTION STATEMENT *(of this Report)*

Approved for public release; distribution unlimited.

17. DISTRIBUTION STATEMENT *(of the abstract entered in Block 20, if different from Report)*

18. SUPPLEMENTARY NOTES

19. KEY WORDS *(Continue on reverse side if necessary and identify by block number)*

Interferometer
Optical Diagnostics
Astigmatism Measurement
Focus Measurement
Beam Quality Measurement

20. ABSTRACT *(Continue on reverse side if necessary and identify by block number)*

A method has been developed for determining the Optical Transfer Function of a coherent optical system by edge scanning a focused output sample of the system across a detector to obtain the Edge Response Function. This Function is then electronically differentiated and Fourier Transformed to yield the Optical Transfer Function and the Point Spread Function. Experimentally generated Edge Response Functions, Line Spread Functions, Optical Transfer Functions, and Point Spread Functions were compared to theoretical

DD FORM 1473 EDITION OF 1 NOV 65 IS OBSOLETE

contd

SECURITY CLASSIFICATION OF THIS PAGE(When Data Entered)

BLOCK 20:

predictions for a laboratory HeNe optical system and excellent agreement
was obtained. Applications of this technique to laser beam control
systems are discussed.

SECURITY CLASSIFICATION OF THIS PAGE(When Data Entered)

i (a)

This final report was prepared by the Air Force Weapons Laboratory, Kirtland Air Force Base, New Mexico under Job Order 00011497. Major O'Neil (LRO) was the Laboratory Project Officer-in-Charge.

When US Government drawings, specifications, or other data are used for any purpose other than a definitely related Government procurement operation, the Government thereby incurs no responsibility nor any obligation whatsoever, and the fact that the Government may have formulated, furnished, or in any way supplied the said drawings, specifications, or other data is not to be regarded by implication or otherwise as in any manner licensing the holder or any other person or corporation or conveying any rights or permission to manufacture, use, or sell any patented invention that may in any way be related thereto.

This technical report has been reviewed and is approved for publication.

BURTON D. O'NEIL
Major, USAF
Project Officer

ROY L. PARNELL
Captain, USAF
Optical Engineer

DAVID F. HOLMES
Civilian
Electrical Engineer

LAWRENCE SHER
Chief, ALL Beam Control Branch

DEMOS T. KYRAZIS
Colonel, USAF
Chief, Laser Development Division

This report has been reviewed by the Information Office (OI) and is releasable to the National Technical Information Service (NTIS). At NTIS, it will be available to the general public, including foreign nations.

i (b)

CONTENTS

ILLUSTRATIONS

ILLUSTRATIONS (Continued)

SECTION I   INTRODUCTION

This TR documents the theory, development, and operation of
the Air Force Weapons Laboratory (AFWL) Scanning Interferometer.
The theory behind the Scanning Interferometer (refs. 1 and 2) is briefly
discussed along with computer plots of expected results. Then the ex-
perimental configuration used at the AFWL is presented along with the
results obtained for various degrees of defocusing aberrations. The
TR is concluded with a brief discussion of conclusions and potential
applications of the Scanning Interferometer to optical system measurement.

SECTION II THEORETICAL BACKGROUND

The following is a brief discussion of the theoretical basis for the Scanning Interferometer. First, the formalization for the normalized Point Spread Function, or Impulse Response, of an optical system is developed. Then it is shown how this Impulse Response can be scanned to yield an Edge Response which can be mathematically manipulated to yield the Optical Transfer Function (OTF) of the optical system.

Figure 1 is a typical aperture imaging system where x, y is the object plane, a, b is the aperture plane, and x',y' is the image plane. Let a limiting ray from the axial point 0 of the object intersect the aperture plane at a height R. Other rays are devoted with rectangular coordinates a,b in the aperture plane by the normalized coordinate

$$\xi = \frac{a}{R} \quad , \quad \eta = \frac{b}{R}$$

The complex amplitude, $\psi(x',y')$, in the image plane due to a point source located at x ,y in the object plane is given by the Fresnel-Kirchoff diffraction integral over the normalized aperture

$$\psi(x',y') = \frac{-iAR^2}{\lambda} \iint_{A_0} \frac{e^{ik(h+f)}}{hf} \left[\frac{\cos\ (nh)\ -\ \cos\ (nf)}{2} \right] d\xi d\eta \quad (1)$$

where
$$K = \frac{2\pi}{\lambda}$$

The quantity A is the amplitude of the point source, R is the radius of the aperture, λ is the wavelength of the light, the quantity in brackets is the obliquity factor which is never greater than unity nor less than zero, h is the distance from the source to a point in the aperture plane, and f is the distance from the aperture plane to the image plane.

The paraxial approximation is made based on the assumptions that the distances z_1 and z_2 are much greater than the maximum linear dimension of the aperture, and that in both the object and image planes only a small region about the z axis is of interest so that the distances z_1 and z_2 are much greater than the maximum linear dimension of these regions. Thus, the obliquity factor is set to unity and the quantities h and f in the denominator of equation (1) equal z_1 and z_2 , respectively. The quantity h+f in the exponent, on the other hand, is very sensitive to small changes in f and h and approximations must be made very carefully.

To simplify the exponential, the Fresnel approximation of replacing the quantities h and f by the first two terms of their respective binomial expansion is used. Upon substituting and algebraically rearranging the exponential, we have:

$$\psi(u'v'.v_o v_o) = D \int_{-1}^{1} \int_{-1}^{1} e^{-\frac{ikR^2}{2}(\frac{1}{Z_1} + \frac{1}{Z_2})(\xi^2+\eta^2)} e^{-i2\pi\left[\xi(u'+u_o)+\eta(v'+v_o)\right]} d\xi d\eta$$
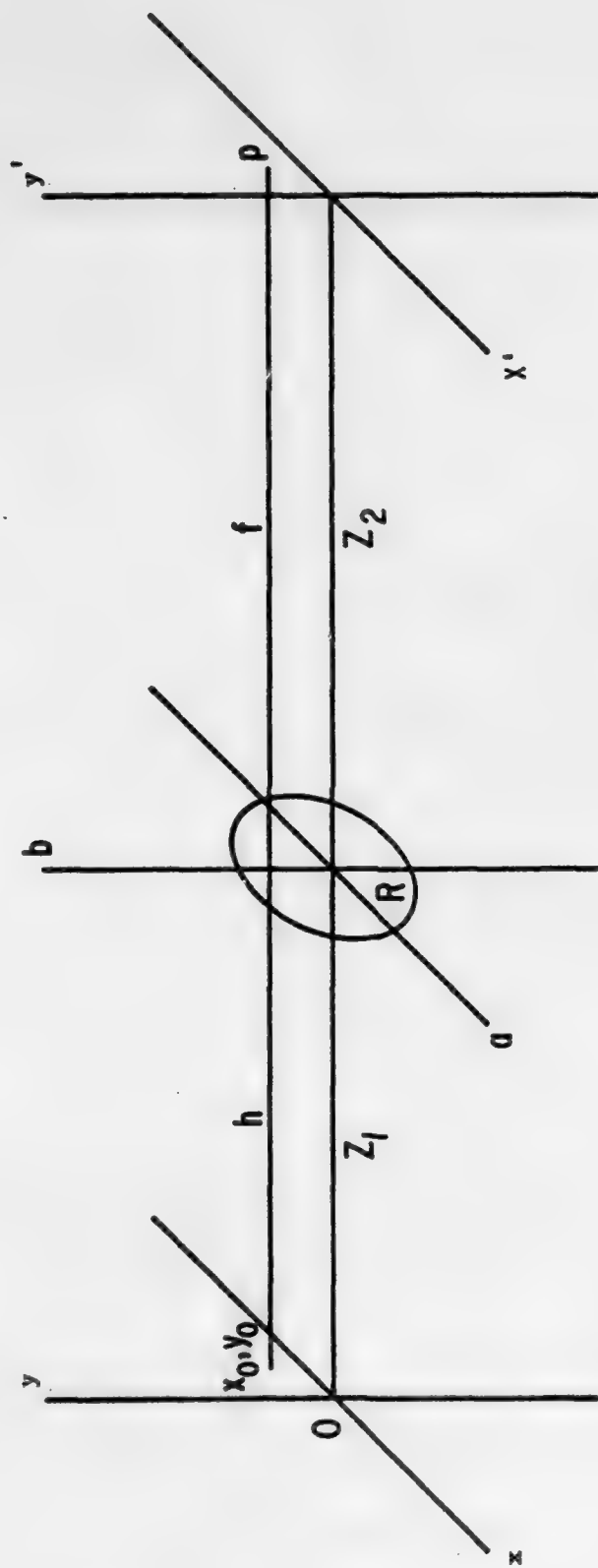$$(2)$$

Figure 1. Typical Aperture Imaging System

Where D is defined by:

$$D = \frac{-iAR^2}{\lambda Z_1 Z_2} \; e^{-ik \left\{ (Z_1+Z_2) + \frac{1}{2} \left[(\frac{u'\lambda}{R})^2 + (\frac{v'\lambda}{R})^2 + (\frac{u_0\lambda}{R})^2 + (\frac{v_0\lambda}{R})^2 \right] \right\}}$$

Also defined are the normalized coordinates in the object plane

$$u_0 = \frac{x_0 R}{\lambda Z_1} \qquad\qquad v_0 = \frac{y_0 R}{\lambda Z_1}$$

and in the image plane

$$u' = \frac{x'R}{\lambda Z_2} \qquad\qquad v' = \frac{y'R}{\lambda Z_2}$$

Thus, equation (2) can be rewritten as:

$$\psi(u'v',u_0 v_0) = D \int_{-1}^{1}\int_{-1}^{1} A(\xi, \eta) \; e^{-i2\pi \left[\xi(u'+u_0) + (v'+v_0) \right]} \, d\xi d\eta \qquad (3)$$

where the aperture function $A(\xi,\eta)$ is equal to the unitary phase factor $g(\xi,\eta)$:

$$g(\xi,\eta) = e^{\frac{-ikR^2}{2} \left[(\frac{1}{Z_1} + \frac{1}{Z_2}) (\xi^2+\eta^2) + \frac{1}{f} \right]} \qquad (4)$$

where ξ,η are within the aperture and $g(\xi,\eta) = 0$ otherwise. At this point in equation (4), we have introduced an imaging element. This element has a focal length f. The new aperture function $g(\xi,\eta)$ now contains the $1/f$ term. From this point on, we are considering an imaging system with well defined conjugate object I_0 and image I_i planes. $(u'v', u_0 v_0)$ is, within the constant D, the Fourier Transform of $g(\xi,\eta)$.

Our system is linear and the quantity $|\psi(u'v',u_0 v_0)|^2$ represents the unnormalized Point Spread Function of our imaging system. The normalized Point Spread Function, or Impulse Response, of our system due to a point source located at x_0, y_0 in the image plane is defined to be:

$$S(u'v',u_0 v_0) = \frac{|\psi(u'v',u_0 v_0)|^2}{\iint |\psi(u'v',u_0 v_0)|^2 \, du' dv'} \qquad (5)$$

4

The denominator represents the total energy in the point spread function and is equal to $|D|^2 A_\rho$. A_ρ is the area of the unnormalized pupil. Thus:

$$S(u'v', u_0 v_0) = \frac{1}{\pi} \left| \int\limits_{-1}^{1}\int\limits_{-1}^{1} g(\xi, \eta) e^{-i2\pi \left[\overline{\underline{d}(u'+v_0) + \xi(v'+v_0)} \right]} d\xi d\eta \right|^2 \quad (6)$$

This equation clearly relates the normalized Point Spread Function to the normalized variables of this imaging system.

Having defined the Impulse Response, the Edge Response Function is now defined and its relation to the MTF is shown. Recall that the image distribution for an extended object is given by the convolution integral (ref. 1):

$$I_i(u'v') = \iint\limits_{-\infty}^{\infty} I_0(u_0 v_0) S(u_0 + u', v_0 + v') du_0 dv_0 \quad (7)$$

Let the object distribution be independent of the y direction. Then:

$$I_i(u') = \int\limits_{-\infty}^{\infty} I_0(u_0) h(u_0 + u') dv_0 \quad (8)$$

where $I_0(u) = 1$ when $u = o$
$I_0(u) = o$ otherwise

Next, the Line Spread Function $h(u')$ is introduced:
$$h(u') = \int\limits_{-\infty}^{\infty} S(u'v') dv' \quad (9)$$

For the deviation of equations (8) and (9), see the appendix.

We infer that the frequency response of this system to one dimensional objects is the Fourier Transform of the Line Spread Function (ref. 3):

$$S(u_0) = \int\limits_{-\infty}^{\infty} h(u') e^{i2\pi u_0 u'} du' \quad (10)$$

Where u_0 is the normalized spatial frequency variable and represents a sinusoidal contrast object independent of the y direction,

$$I_0(u_0) = Sin(u_0). \quad (11)$$

Now consider an edge oriented parallel to the y' axis in the image plane. The integrated flux of the point spread function which passes the edge as of function of spatial position x' is called the Edge Response Function.

5

$$E(u') = \int_{u'=-\infty}^{u'} h(u')du' = \int_{-\infty}^{u'} \left(\int_{-\infty}^{\infty} S(u',v')dv' \right) du' \qquad (12)$$

Using the above double integral representation, i.e., the Edge Response Function, the edge sums in the y' direction at a particular x'. Solving the inner integral then moves to a new x' which complies with the requirements of the outer integral. There obviously exists a simple relationship between the Line Spread Function h(u') and the Edge Response Function E(u) namely:

$$h(u') = dE(u)/du'. \qquad (13)$$

Thus, the measured Edge Response Function can be differentiated to determine the Line Spread Function. A Fourier Transform of the Line Spread Function gives the OTF perpendicular to the edge of the optical system under test. (Refs 2 and 3)

Computer codes to model the above and to produce point spread functions, line spread functions, Edge Response Functions and OTF's have been developed. Figures 2 through 11 show some of these functions for varying degrees of defocusing aberrations present in the aperture function.

Figures 2 through 6 are the point spread functions for varying amounts of defocus. All the peak intensities are normalized to 1 which is the maximum value of the perfect (zero defocus) point spread function (figure 2). These figures may be compared with figure 16 which shows actual photographs of experimentally produced point spread function. Figure 11 shows the predicted Edge Response Functions (ERF) all normalized to the same integrated energy in the point spread function. Only figure 17 shows the experimental ERF for a perfect beam. The predicted line spread functions (LSF) of figures 7 through 11 may be compared with the experimentally derived LSF of figures 17 through 21. Here one sees excellent agreement between theory and experiment. Finally, the predicted OTF's (figure 13) can be compared to the experimental OTFs of figures 22 through 27. Here again there is good agreement with any discrepancies due to the difficulty in obtaining pure defocus of the desired degree uncoupled with other aberrations, primarily astigmatism.
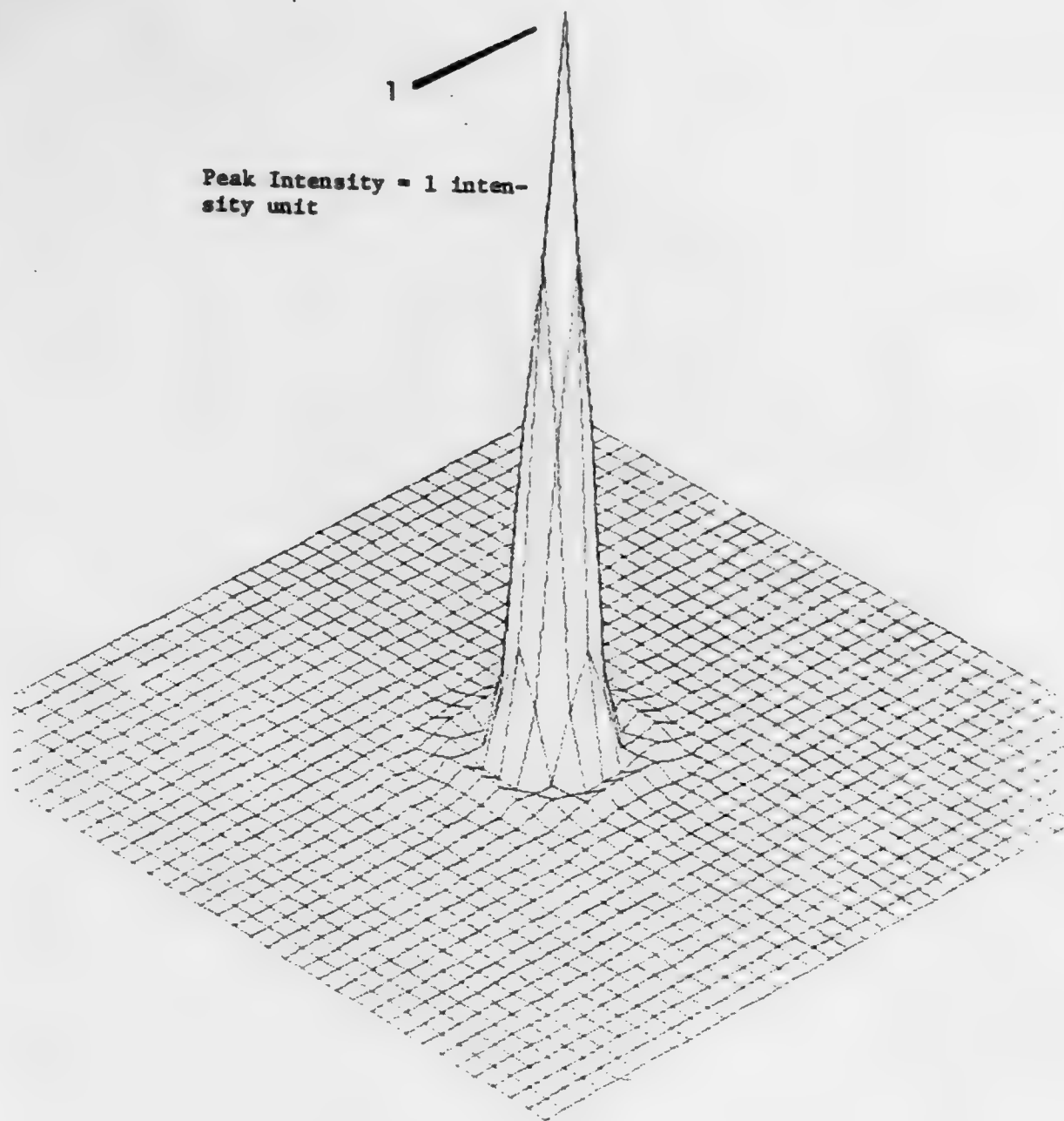
Peak Intensity = 1 intensity unit

Figure 2. Computer Point Spread Function, Perfect Beam

0.41

Peak Intensity = 0.41
Intensity Units
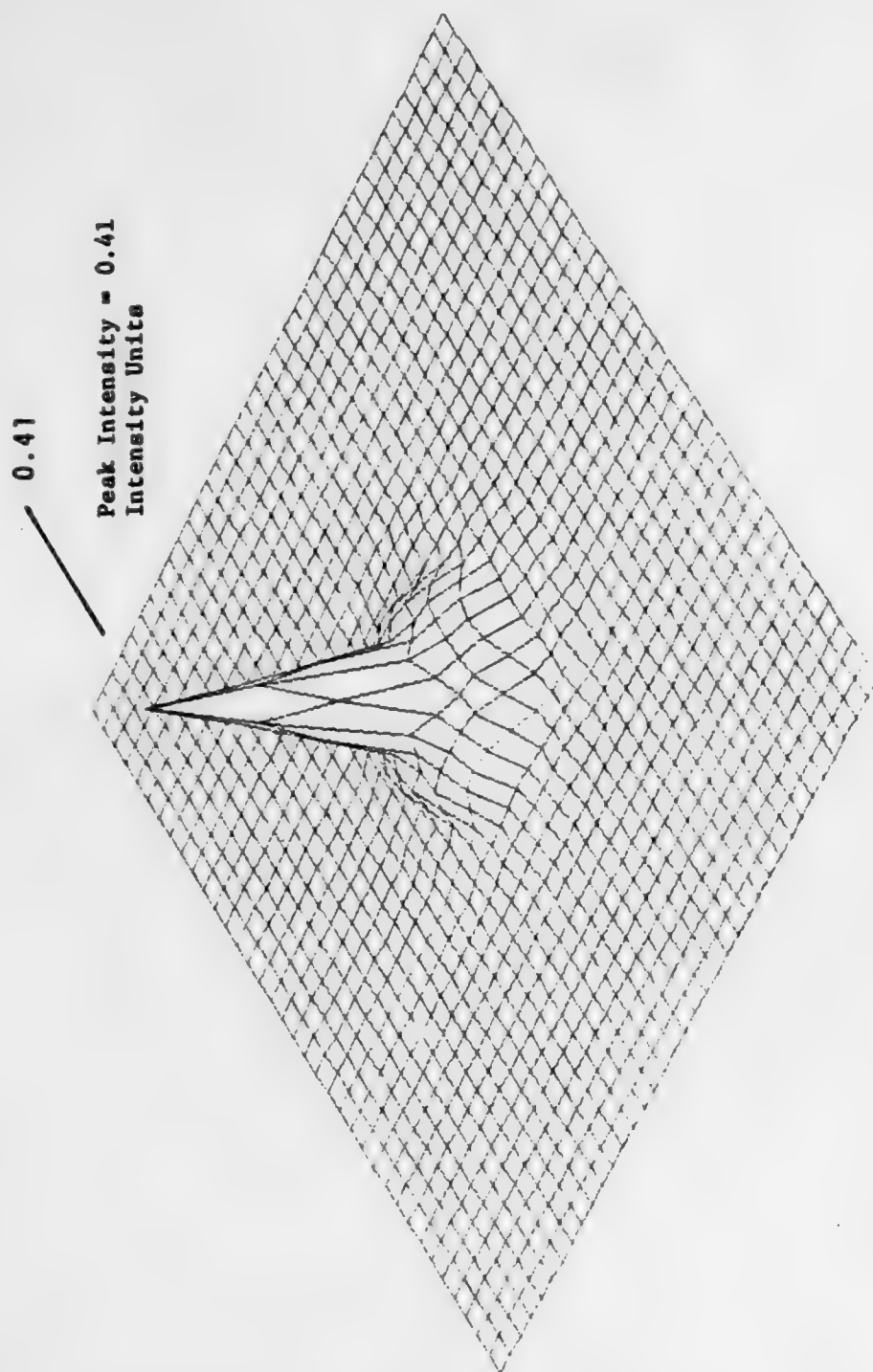
Figure 3. Computer Point Spread Function, 1/2 Wave Defocus

0.05

Peak Intensity = 0.05
Intensity Units
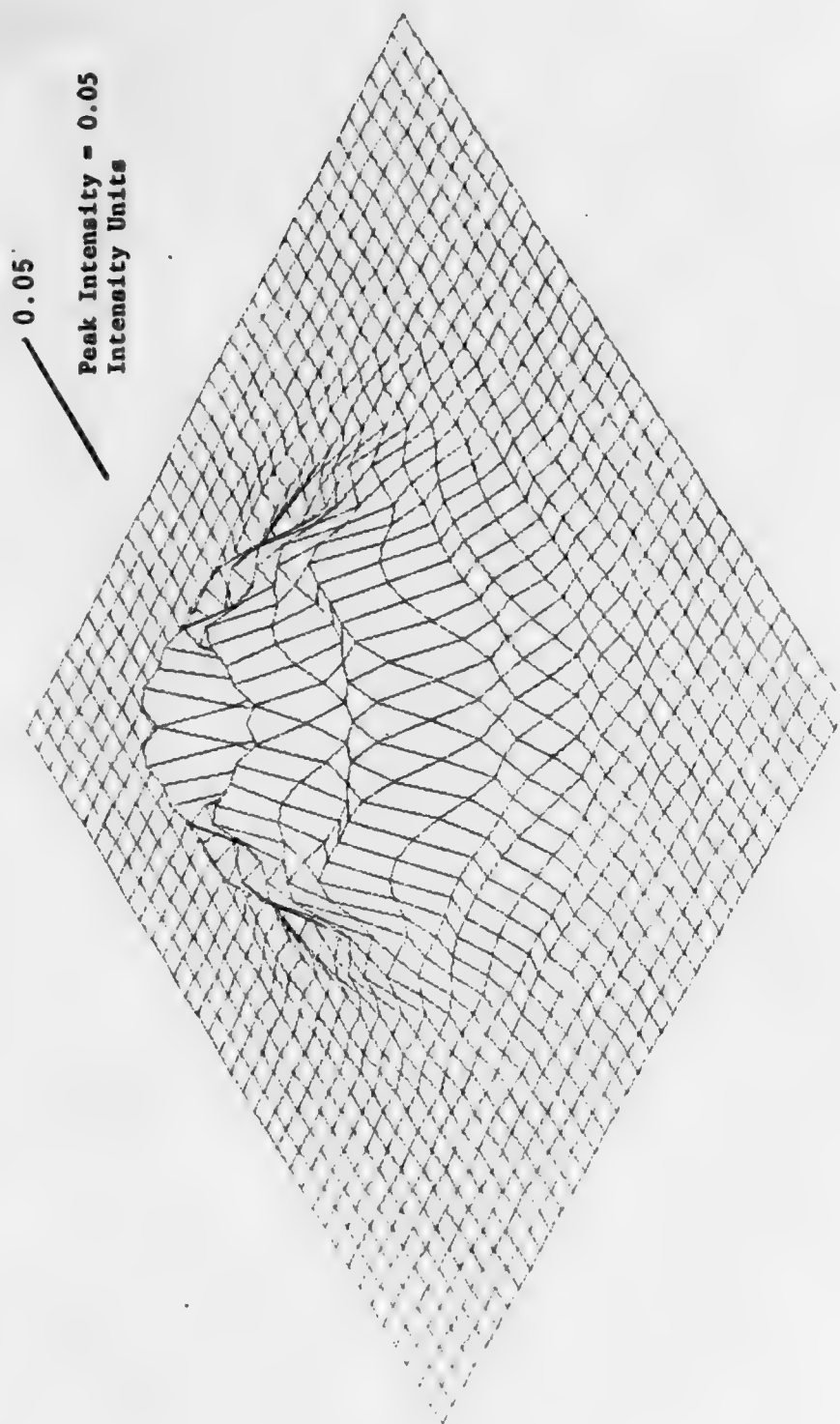
Figure 4. Computer Point Spread Function, 1 Wave Defocus

0.04

Peak Intensity = 0.04
Intensity Units
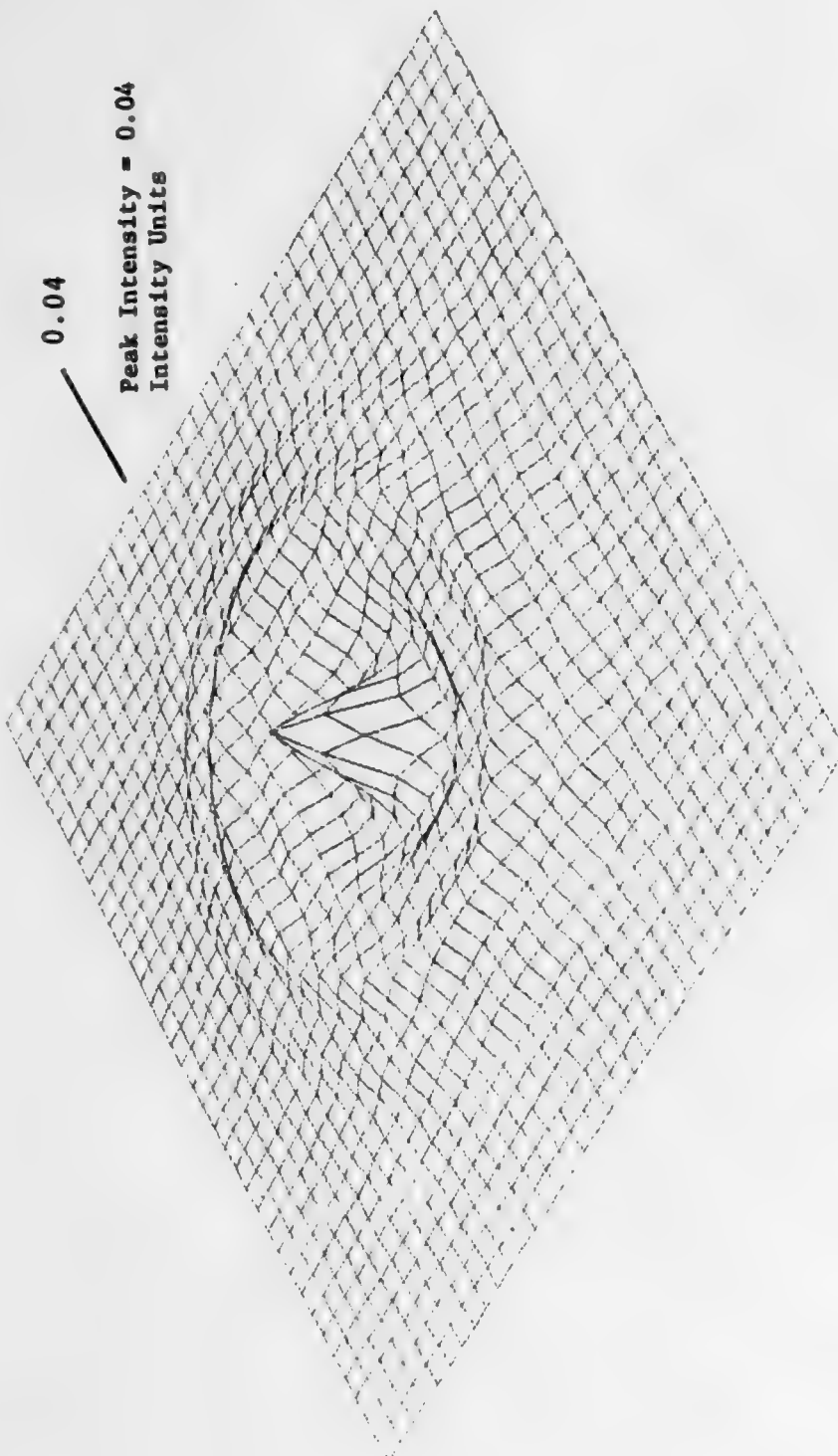
Figure 5. Computer Point Spread Function, 3/2 Wave Defocus

Peak Intensity = 0.01
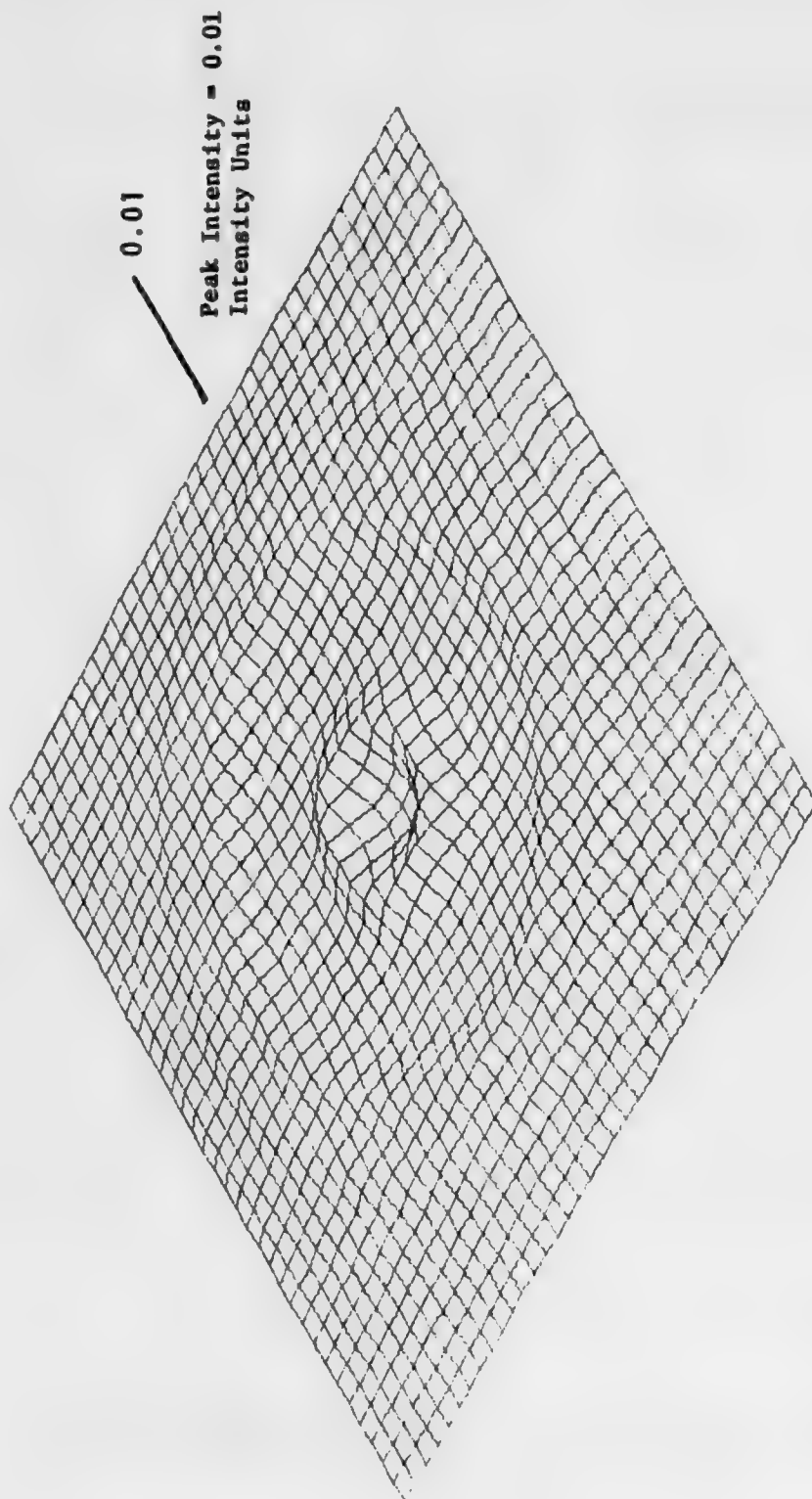Intensity Units

0.01

Figure 6. Computer Point Spread Function, 2 Wave Defocus
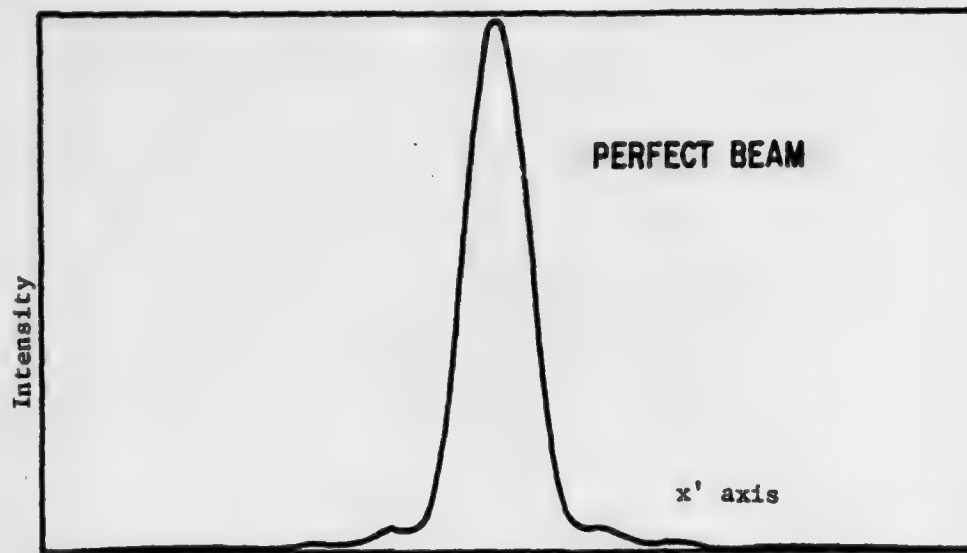
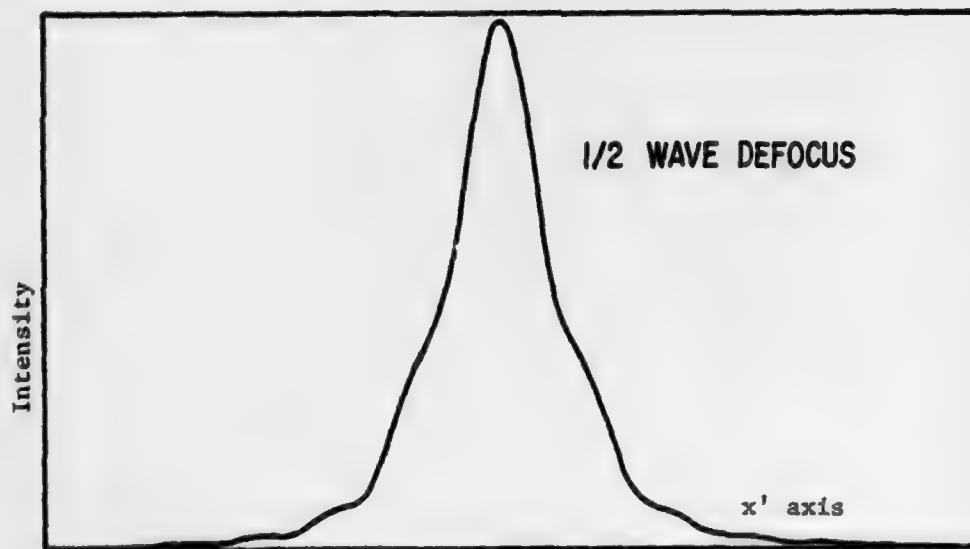Figure 7:   Computed Line Spread Function

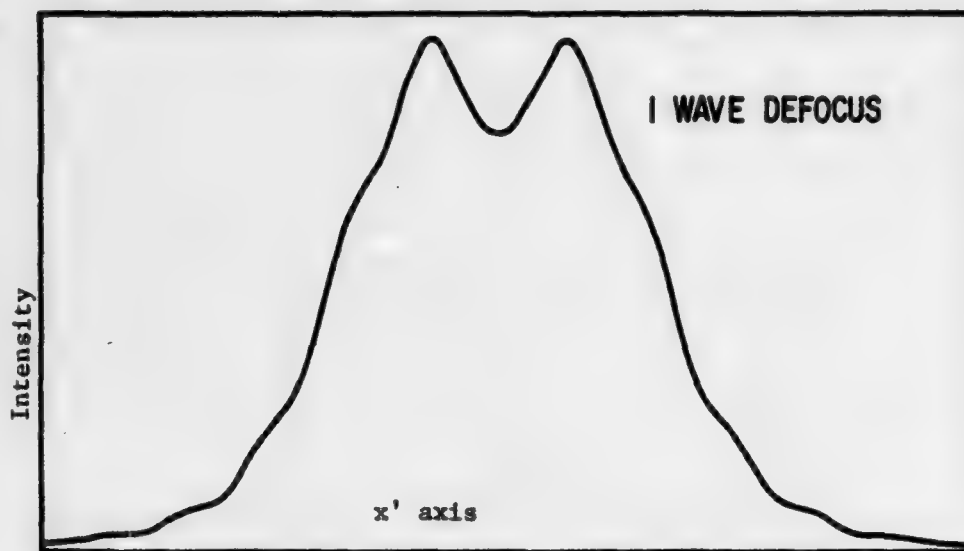Figure 8:   Computer Line Spread Function
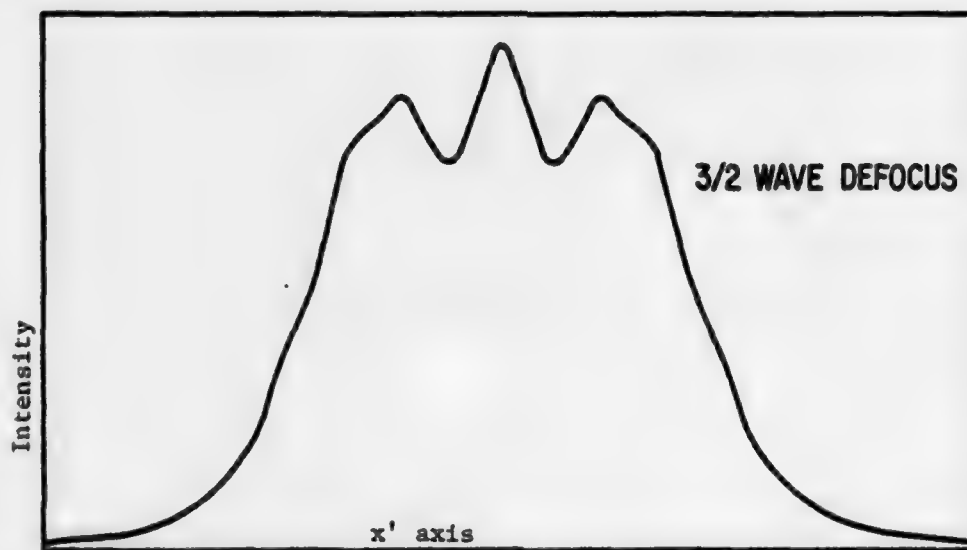
Figure 9: Computed Line Spread Function

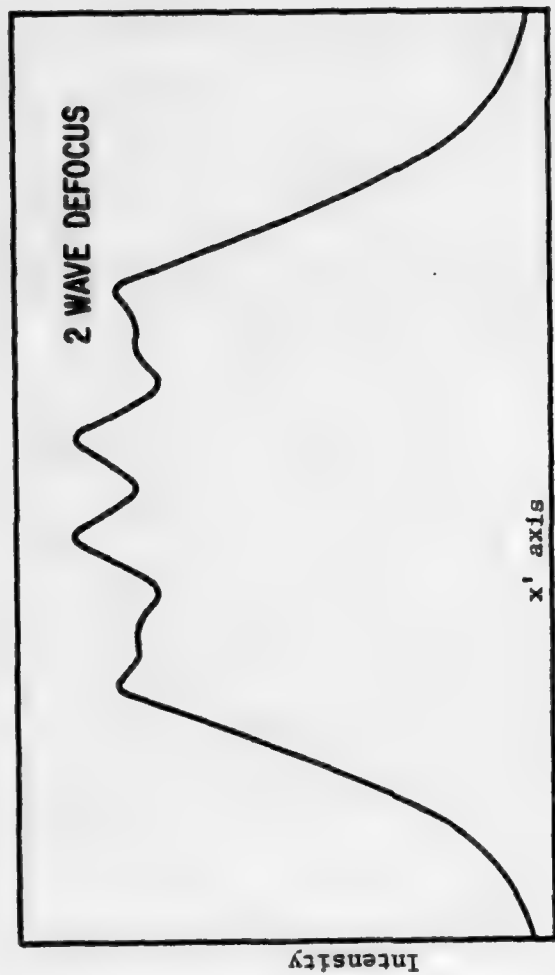Figure 10: Computed Line Spread Function

13

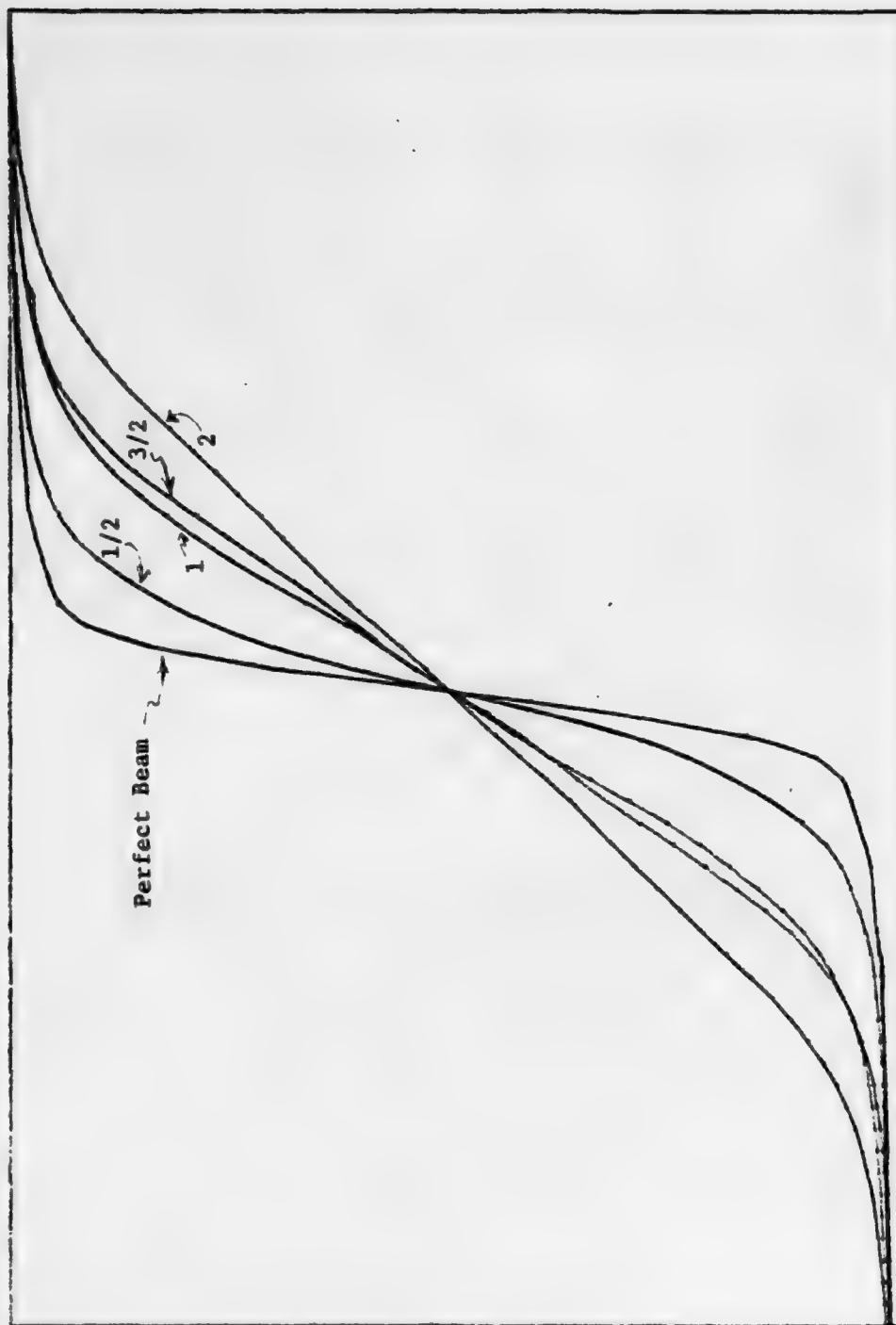Figure 11. Computer Line Spread Function

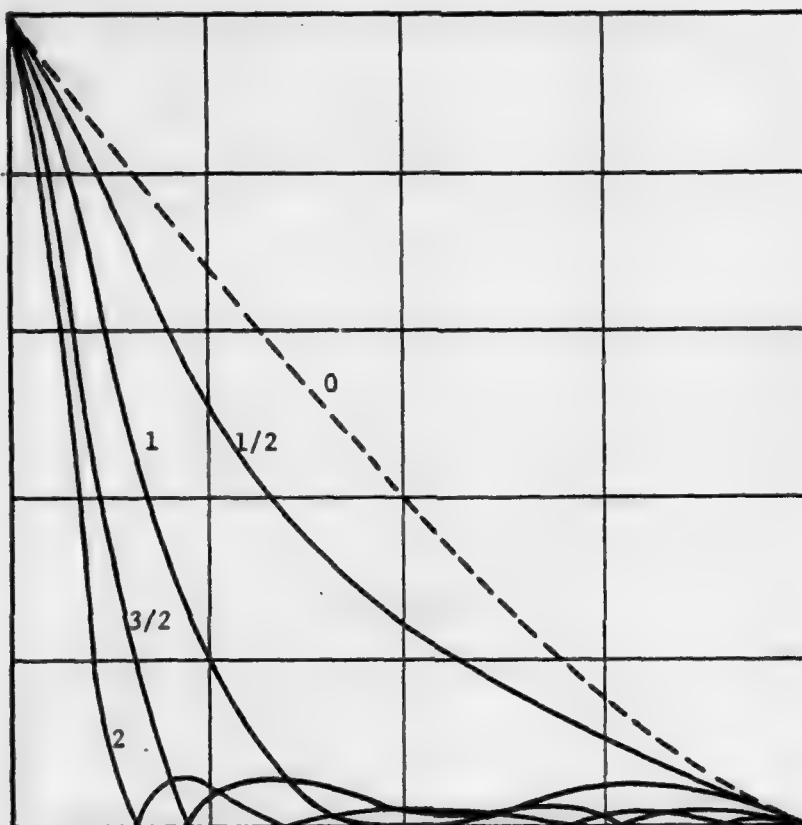Figure 12. Computed x' Axis Edge Response Functions

15

Figure 13. Computed Optical Transfer Functions

SECTION III

EXPERIMENTAL CONFIGURATION

The layout of the AFWL Scanning interferometer is shown below in figure 14. The electronics block diagram is shown in figure 15. The HeNe laser beam from the laser is expanded to a 150 mm diameter by a Tropel Model 280-150 beam expander. Then, to further insure input beam quality, the expanded beam is apertured to a 25 mm diameter before being passed through a diffraction limited 150 mm diameter focusing lens. After passing through the lens, the beam strikes the scanning mirror prior to reaching focus at the quadrant detector. The scanning mirror scans the beam in any desired axis across the detector and the output of the detector is the Edge Response Function. The Edge Response Function is then electronically differentiated to yield the Line Spread Function which is then digitized and sent on to a PDP-11 computer. In the computer, the Fourier Transform of the digitized Line Spread Function is obtained and this transform is the Optical Transfer Function of the system.

Prior to operation of the Scanning Interferometer, a microscope objective is placed at the focus of the lens so that the Airy Disk pattern can be examined. Then the optical system is adjusted to insure that the initial input beam is aberration free.
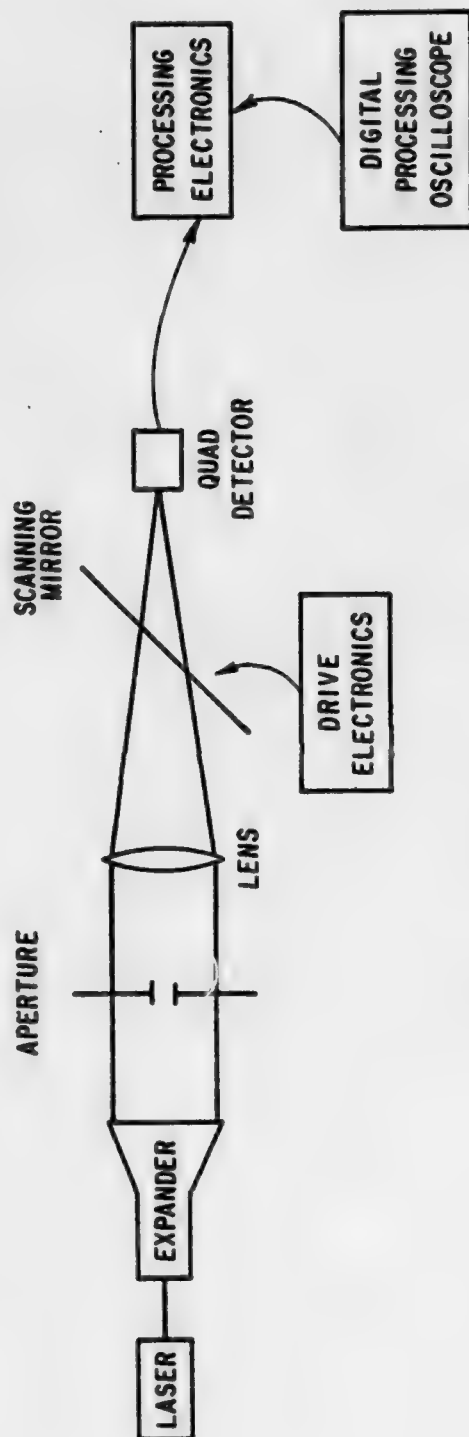
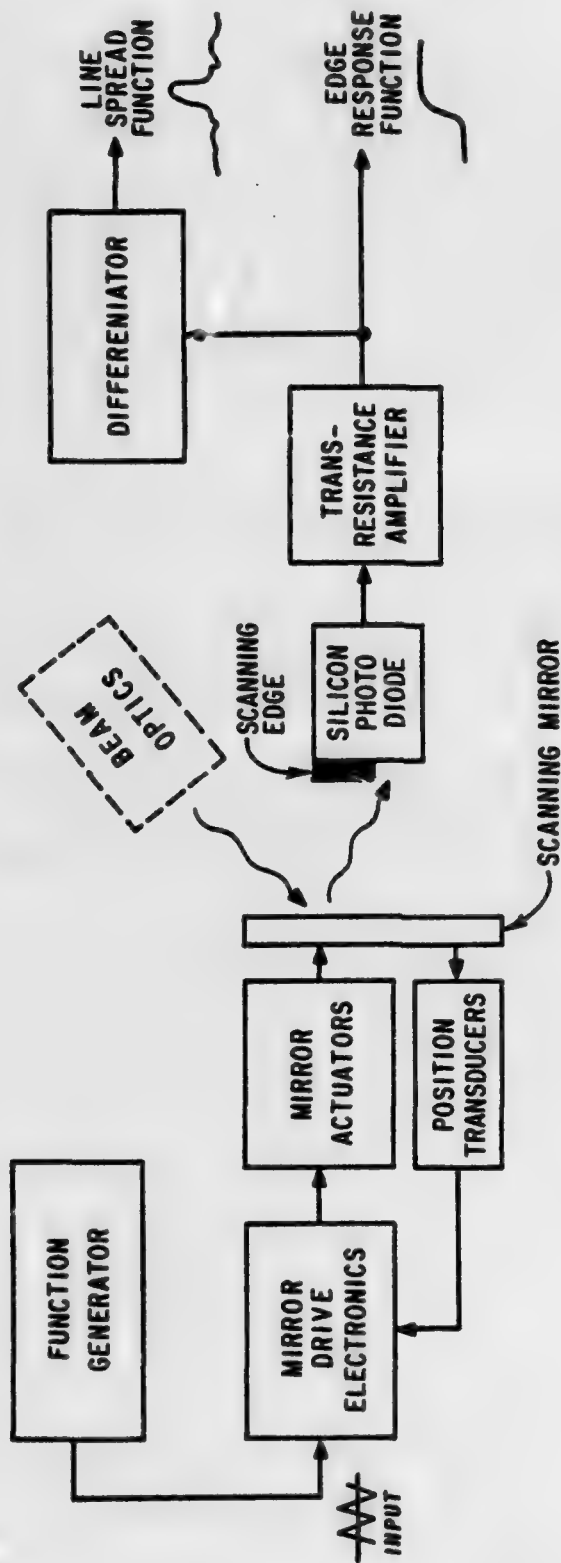Figure 14. Scanning Interferometer

Figure 15. Scanning Interferometer Electronic Block Diagram

19

SECTION IV

EXPERIMENTAL RESULTS

Typical Airy Disk patterns are shown in figure 16 for beams with defocus aberratons of 1/2, 1, 3/2, and 2 wavelengths. The theory predicts that for 1 and 2 wavelengths of defocus, the intensity on axis of point spread function is zero which agrees with the experimentally observed PSFs, figure 16. One sees that for the 1 wavelength PSF, the measured LSF shows a minima on axis and the computed also shows this minima. From the other experimental PSF, one can predict maximas and minimas in the measured LSF and see that they compared exactly with theoretically predicted LSFs. It is instructive to compare the theoretical OTFs of figure 13 with the OTFs generated by Fourier transforming the measured LSFs, figures 22 to 27, for the same degrees of defocusing aberration.

Figure 17 shows the Edge Response Function and the Line Spread Function for an aberration free, "perfect" beam. Figures 18 through 21 show the line Spread Function for defocusing of 1/2, 1, 3/2, and 2 wavelengths.

There is no loss of generality with respect to higher order aberration. Defocusing was chosen since known amounts of defocus could be put into the AFWL laboratory optical system. It is very difficult to put in single higher order aberrations without also coupling into other higher aberrations.

The Fourier Transforms which correspond to these figures are shown in figures 22 through 27 respectively and are summarized in figure 28. All of these figures for the experimental results can be compared with figures 2 through 13 and figure 26 which present the results of theoretical calculations for the same aberrations.
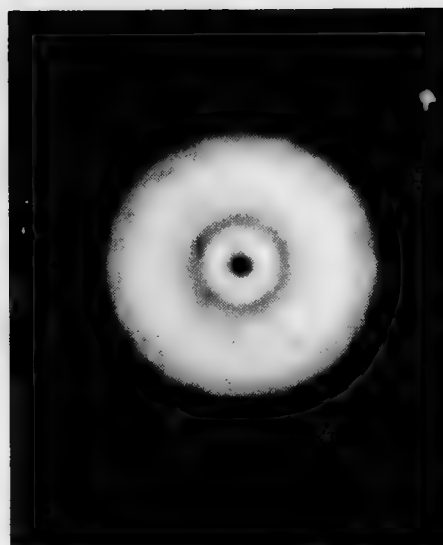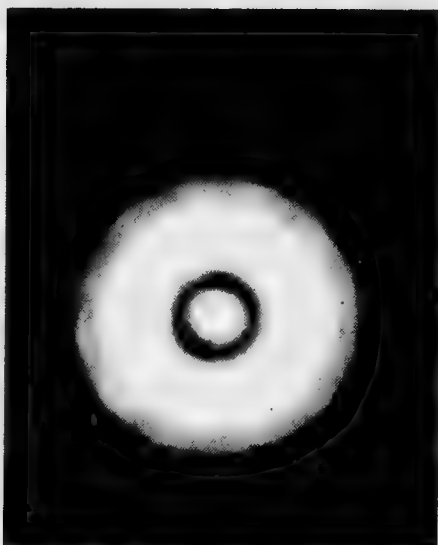
Figure 16:   Experimental Point Spread
            Functions

21
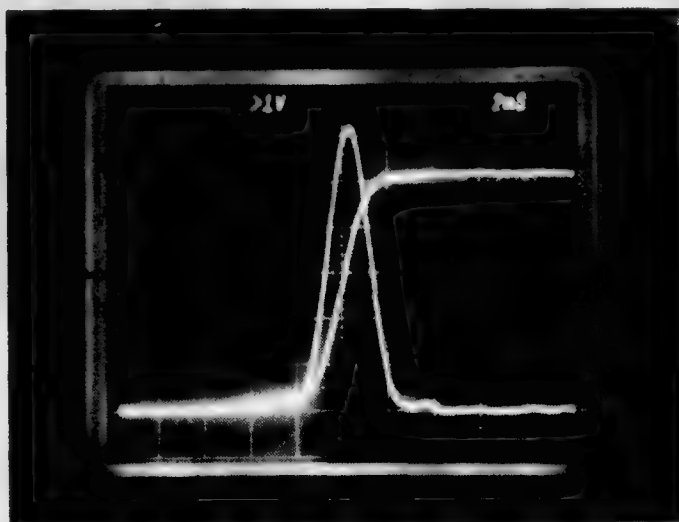
Figure 17. Measured LSF/ERF for Perfect Beam

Figure 18: Measured LSF for 1/2 Wave
Defocus

Figure 19: Measured LSF for 1 Wave
Defocus

Figure 20: Measured LSF for 1 1/2 Wave
Defocus

Figure 21: Measured LSF for 2 Wave
Defocus

Figure 22: Measured OTF for Perfect
Beam

Figure 23: Measured OTF for 1/4 Wave
Defocus

Figure 24: Measured OTF for 1/2 Wave
Defocus

Figure 25: Measured OTF for 1 Wave
Defocus

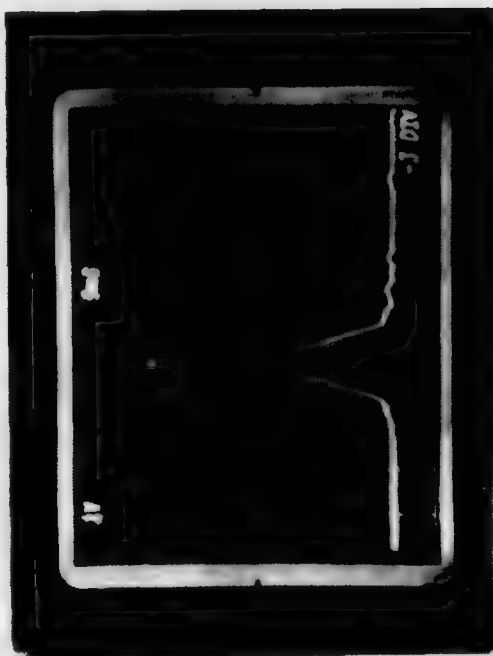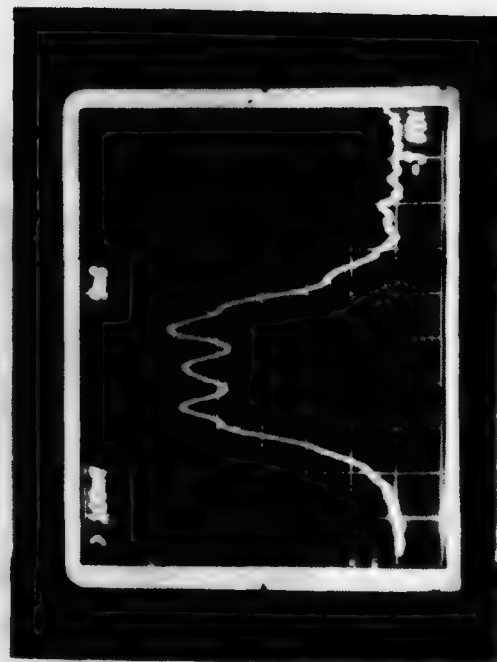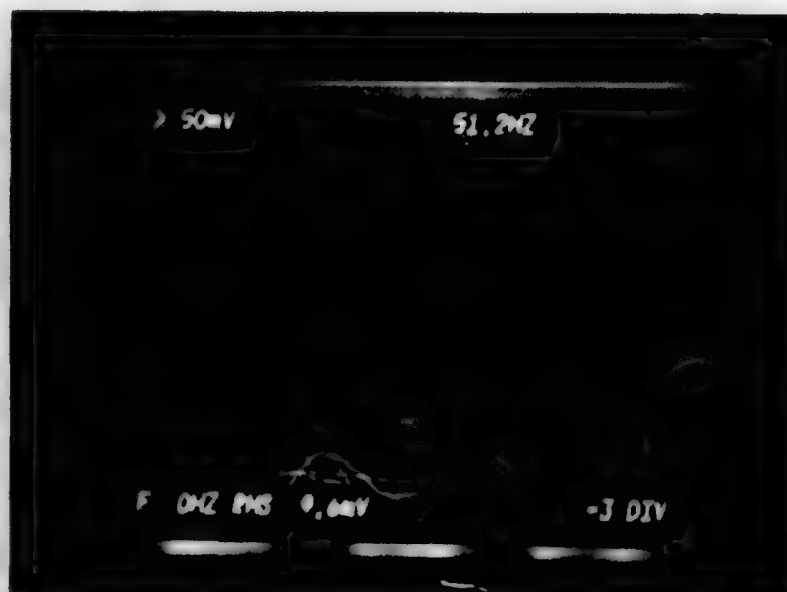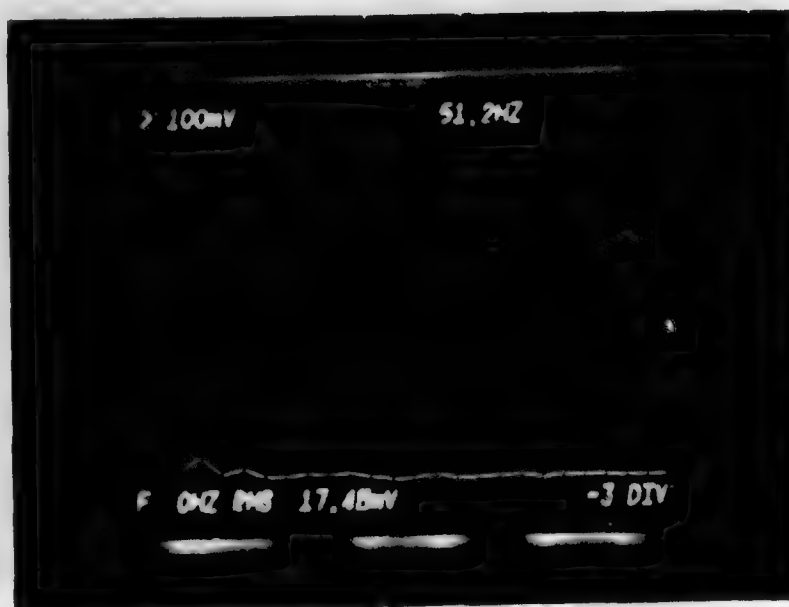**Figure 26:** Measured OTF for 1 1/2 Wave Defocus

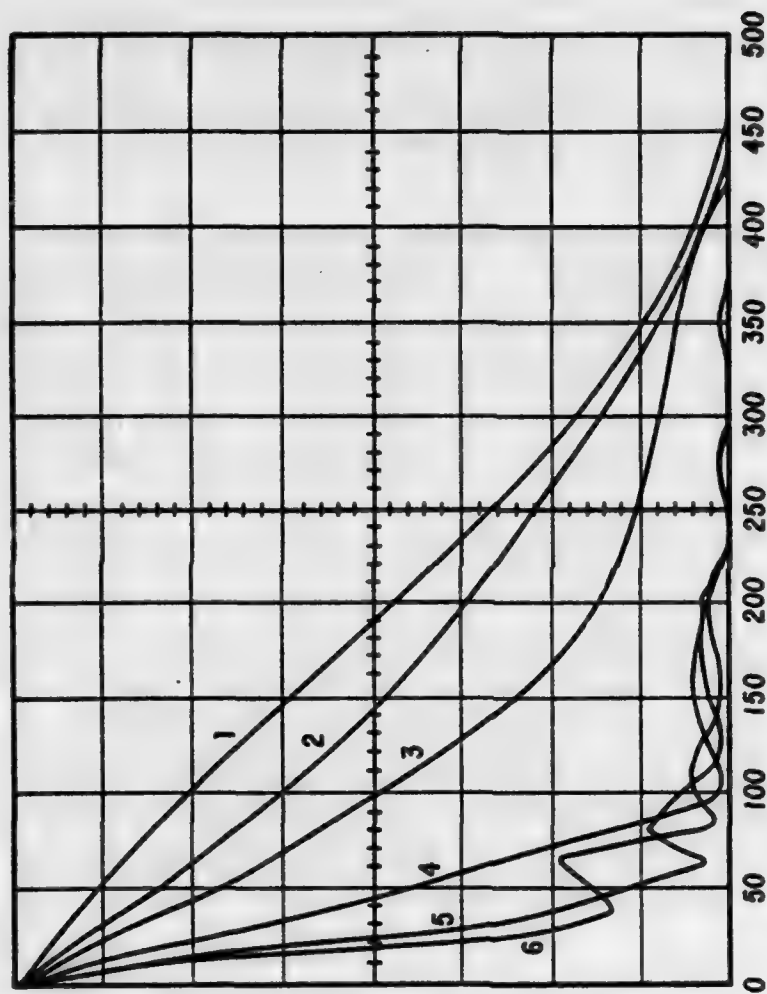**Figure 27:** Measured OTF for 2 Wave Defocus

Figure 28: Modulation Transfer Functions. 1 = Perfect Beam; 2 = 1/4 Wave Defocus; 3 = 1/2 Wave Defocus; 4 = 1 Wave Defocus; 5 = 3/2 Wave Defocus; 6 = 2 Wave Defocus.

27

SECTION V

CONCLUSIONS AND APPLICATIONS

The primary conclusion of these experiments is that the scanning interferometer is a viable tool for determination of the OTF and PSF of an optical system. Since it is virtually impossible to miss an edge, the scanning interferometer showed itself insensitive to misalignment (especially compared to a circular hole scanner). It is very simple and does not require large expensive complicated detector arrays. This is very significant at the far infrared where detectors are not abundant but are expensive. By using a rapidly rotating chopping edge or mirror (as was used in the laboratory setup), ERFs, PSFs and OTFs can be generated from 1 to 4k Hz. If the beam is rotated or the edge is rotated, then two dimensional PSF and OTFs can be generated using a single detector.

Besides being a simple method of finding PSF and OTFs for optical systems, the scanning interferometer technique finds application in diagnosing the far field pattern (PSF) of high energy laser beams. The Cycle III Beam Angle Sensor (BAS) already provides x and y ERFs which are currently wasted information. From this information, the laser far field pattern (PSF) along the x and y axis can be generated in addition to the OTF. A simple modification to the BAS, suggested by Mr. Norbert Schnogg of the Perkin Elmer Corporation, is to rotate the beam into the BAS using a K prism. With the beam rotating, the edge scanner will produce two-dimensional PSF and OTF. A data rate of 300 Hz can easily be accomplished. Laser beam quality measurements can be obtained from the two dimensional PSFs. In addition, if one keeps track (in time) of a moving edge with respect to the detector along the x and y axis one can determine linear tilt information over the full detector field of view. This tilt scheme uses a single detector instead of the expensive quad cell as is currently being used in Cycle III. Thus, in the current BAS the components are already present to determine system OTF along two orthogonal axis and beam quality. These parameters can be determined with only the addition of minicomputer processing and with no major hardware modifications. For Cycle IV, the BAS will incorporate the K prism and provide two-dimensional far field beam quality and linear tilt measurements, (ref. 4). This allows us to remove the current optical diagnostic system saving volume which can now be used for a hog spot tracker.

SECTION VI

FUTURE STUDY AREAS

The ERF slopes become steeper as defocusing decreases, figure 12. By jittering focus on the laser beam into the BAS, it can generate a change in ERF slopes.

AFWL is in the process of studying a series of functions related to the amount of aberration in the aperture function in the following way:

$$S_n \equiv \frac{1}{L_2 - L_1} \int_{L_1}^{L_2} \left| \frac{d^n E(x')}{d^n x'} \right|^2 dx' \qquad n \quad o \qquad (14)$$

$$S_n + 1 \equiv \frac{1}{L_2 - L_1} \int_{L_1}^{L_2} \left| \frac{d^n h(x')}{d^n x'} \right|^2 dx' \qquad n \quad o \qquad (15)$$

where n is an integer,

$E(x')$ = Edge Response Function
$h(x')$ = Line Spread Function
L_1, L_2 are the threshold or gate level.

L_1 and L_2 are important and are variable. A small spot diamter containing the same energy as a large spot diameter will have smaller values of L_1 and L_2. Thus, the shape of the LSF is taken in consideration when determining Sn. The above equation differs from Muller and Buffington, and Ertezas' (ref 5) sharpness index in the following ways:

a. The system is looking at images of a point (point spread function) not extended objects.

b. The basic unit is the edge response function not the intensity distribution of an extended source.

c. Finally, the L_1 and L_2 vary as the point spread function tightens up. Thereby, Sn senses PSF shape which is just as important as slope of the PSF.

Since this scheme is being contemplated to do laser beam clean up, one is interested in the image of a point and the variance from the perfect Airy pattern. One is not interested in extended objects. All lasers appear to eminate from point sources (or more typically aberrated point sources); therefore, it is the PSF and LSFs that are important.

APPENDIX

The basic physical optics imaging equation is:

$$I_i(u',v') = \iint\limits_{-\infty}^{\infty} I_o(u_o,v_o) \, S(u_o + u', \, v_o + v') \, du_o dv_o \tag{A1}$$

where all the variables are defined in the text of this TR. In words, equation (A1) says the image I is equal to the convolution of the object distribution I with the optical system point spread functio 5.

Next, we define the object distribution to be a verticle line independent of the y direction, located at x = o,

where $I_o(u_o) = K$ when $u_o = o$

$I_o(u_o) = o$ otherwise

Now equation (A1) reduces to:

$$I_i(u') = K \int_\infty^\infty S(u', v_o) dv_o \tag{A2}$$

At the conjugate planes of an imaging system, v and v' are not independent but related by paraxial imaging relationships. therefore

and
$$v_o = mv' \tag{A3}$$
$$dv_o = mdv' \tag{A4}$$

m = magnification between object and image.

Using equations (A3) and (A4), equation (A2) is

$$I_i(u') = m \int S(u', mv') dv \tag{A5}$$

Normalizing to unity magnification (i.e., $Z_1 = Z_2$), equation (A5) is
$$I_i(u') = \int_{-\infty}^\infty S(u', v') \, dv' \tag{A6}$$

Equation (A6) is identical to equation (9) in the text and is known as the Line Spread Function h(u'),

$$h(u') = I_i(u') \tag{A7}$$

The imaging equation for a line object is now a one-dimensional convolution

$$I_i(u') = \int_{-\infty}^{\infty} I_o(u_o) \, h(u_o + u') \, du_o \tag{A8}$$

31

Equation (A8) is identical to equation (8) in the text.

Furthermore, since $I_o(u_o)$ has a value only at $u_o = o$, equation (A7) normalized to unity magnification reduces to

$$h(u') = I_i(u') = \int_\infty^\infty S(u',v') \, dv' \qquad (A9)$$

A more rigorous definition of a line object distribution than was used in the above discussion can be obtained by using the Dirac delta function $d(u_o)$ defined as

$$I_o(u_o) = \delta(u_o) \qquad (A10)$$

where $\qquad \delta(u_o) = \begin{cases} \infty & u_o = 0 \\ 0 & \text{otherwise} \end{cases}$

In addition, the function has the following fundamental properties:

$$\int_{-t}^{t} \delta(u_o) \, du_o = 1 \qquad\qquad t \to \infty \qquad (A11)$$

$$\int_{-\infty}^{\infty} h(u_o) \, \delta(u'+u_o) \, du_o = h(u') \qquad (A12)$$

at each point of continuity of $h(u_o)$. The authors feel no further insight into the physics will be obtained by using the Dirac delta function; however, using equations (A9) through (A11) will result in the same definition of the Line Spread Function $h(u')$ as equation (A8).

REFERENCES

1. Goodman, J. W., <u>Introduction to Fourier Optics</u>, McGraw Hill, New York, 1968, pg 19-21.

2. Barakat and Houston, <u>Journal of the Optical Society of America</u>, Vol 54, pg 768, 1964.

3. Tatian, Berge, "Method for Obtaining the Transfer Function Directly from the Edge Response Function", <u>Journal of the Optical Society of America</u>, Vol 55, No. 8, 1965.

4. Final Design Analysis Report, CDRL A010, Contract F29601-76-C-0100, "Cycle IV Upgrade Conceptual Design", 1976, Pratt and Whitney Aircraft, West Palm Beach, Florida.

5. Erteza, Ahmed, "Sharpness Index and its Application to Focus Control", <u>Applied Optics</u>, Vol 15, April, 1976.